



Assessing the nitrate vulnerability of shallow aquifers under Mediterranean climate conditions

Paolo Nasta^{a,*}, Giuliano Bonanomi^{b,c}, Jirka Šimůnek^d, Nunzio Romano^{a,e}

^a Department of Agricultural Sciences, AFBE Division, University of Naples Federico II, Portici, Naples, Italy

^b Department of Agricultural Sciences, BPSAF Division, University of Naples Federico II, Portici, Naples, Italy

^c Task Force on Microbiome Studies, University of Naples Federico II, Naples, Italy

^d Department of Environmental Sciences, University of California Riverside, CA, USA

^e The Interdepartmental Center for Environmental Research (C.I.R.A.M.), University of Naples Federico II, Naples, Italy

ARTICLE INFO

Handling Editor: Dr. Z. Xiyang

Keywords:

Groundwater
Nitrate leaching
Root uptake
Transit time distribution (TTD)
Hydrus-1D
HYPRES database
Campania

ABSTRACT

The EU Nitrates Directive calls for urgent integration of process-oriented indicators of nitrate fate with map overlay approaches for assessing nitrate vulnerable zones (NVZs). In the region of Campania (southern Italy), groundwater contamination represents a serious concern because of the presence of intensive agricultural practices and livestock farming. A protocol was proposed to assess the probability distribution of the following three indicators of nitrate transport across the vadose zone: *i*) annual cumulative nitrate flux entering the shallow aquifer, *ii*) annual cumulative root nitrate uptake, and *iii*) nitrate transit time across the vadose zone. This method involves numerical simulations of soil water flow and solute transport using Hydrus-1D for a representative 10-m-thick soil profile beneath an irrigated maize plot located in a study area within the Sele plain, Campania. Two scenarios are built by running a set of one hundred (20-yr-long) simulations at a daily time resolution: *i*) 195 kg N ha⁻¹ of nitrate fertilizer (urea) is applied annually to estimate the probability distributions of annual cumulative nitrate leaching and root nitrate uptake (Scenario 1), *ii*) 195 kg N ha⁻¹ of nitrate fertilizer (urea) is applied once to estimate the nitrate transit time distribution across the soil profile (Scenario 2). In each Scenario, the simulations consider two agricultural practices with either one or three annual nitrate fertilizer applications subject to randomly generated climate forcing using a Monte Carlo approach. Variations in soil and rainfall properties are described by the Miller-Miller geometric similitude and the Poisson parameterization, respectively.

In Scenario 1, roots absorb on average 80.3 kg N ha⁻¹ every year (corresponding to 40% of applied nitrate), and the median annual cumulative nitrate flux across the soil profile bottom is 74.9 kg N ha⁻¹ (representing about 38% of applied nitrate) when urea is applied in a single treatment. In contrast, when fertilizer is applied in three treatments, 112.4 kg N ha⁻¹ (corresponding to almost 60% of applied nitrate) of nitrate is removed by root water uptake, and the median annual cumulative nitrate leaching is 52.4 kg N ha⁻¹ (corresponding to about 27% of applied nitrate). In Scenario 2, mean transit time values are 2741 days, 2707 days, and 2650 days when urea is applied on April 1st, June 1st, and August 1st, respectively. Our model simulations provide useful indicators of nitrate transport and can be integrated with map overlay procedures for delineating nitrate vulnerable zones.

1. Introduction

The agri-food system is one of the main socio-economic sectors in Campania, a region of southern Italy where the most productive areas extend over the internal and coastal alluvial plains with rather intensive agricultural practices. Campania is also a renowned region worldwide for the breeding of buffaloes to produce mozzarella cheese and other

excellent dairy products. Extensive fertilizers and animal manure applications boost crop production at the cost of polluting the environment (Infascelli et al., 2009). The rapid deterioration of groundwater quality observed throughout the world over the last decades represents a serious concern, particularly in Campania, where great attention is devoted to the transport toward shallow aquifers of potentially toxic elements (PTEs) that are detrimental to human health. For this reason, European

* Corresponding author.

E-mail address: paolo.nasta@unina.it (P. Nasta).

<https://doi.org/10.1016/j.agwat.2021.107208>

Received 29 April 2021; Received in revised form 21 July 2021; Accepted 22 September 2021

Available online 5 October 2021

0378-3774/© 2021 Elsevier B.V. All rights reserved.

Union (EU) policies aim at protecting shallow aquifers by promoting sustainable land management, whose efficiency is entrusted to a reliable mapping of groundwater vulnerability (Mylevaganam and Ray, 2016; Wall et al., 2020). Vulnerability can be conceptualized in different ways, but in this study, we follow the definitions given by National Research Council (1993) that groundwater vulnerability is viewed as the ease with which a PTE applied on (or near) the land surface can migrate to the aquifer under a given set of agricultural agronomic practices, contaminant characteristics, and hydrogeological sensitivity conditions.

In most cases, and especially with the help of Geographic Information System (GIS) tools, widespread approaches are based on mapping topographic, hydrogeological, pedological, land-use features controlling the propagation of PTEs through the unsaturated and saturated zones. Scores and weights are assigned to the various environmental factors to obtain classes of groundwater vulnerability to contamination from a certain source following a map overlay procedure (Doerfliger et al., 1999; Rupert, 2001; McLay et al., 2001; Antonakos and Lambrakis, 2007). The parameter weighting and rating approaches (also known as Point Count System Models; e.g., DRASTIC, SINTACS) can be easily employed in large-scale applications, but express groundwater vulnerability in a rather empirical way and show the effect of a certain degree of subjectivity (Van Stempvoort et al., 1993; McLay et al., 2001; Panagopoulos et al., 2006; Huan et al., 2012). In contrast, the use of a process-oriented model, simulating water flow and solute transport in the porous media, enables effective indicators (sometimes also referred to as “functional performance indicators”) of PTE transport to be identified. This represents a step forward and a more objective and efficient method to assess groundwater vulnerability, especially for shallow aquifers. However, the prediction performance of these types of models is highly dependent on the quantity and quality of information on input data and system properties. It seems still rather unfeasible to assess the groundwater vulnerability over relatively large spatial scales by using three-dimensional (3D) process-oriented hydrological models. However, a viable way to provide details about solute transport is to implement one-dimensional (1D) models in spatially representative soil profiles of the area of interest.

The Nitrates Directive 91/676/EEC (reiterated by the new 2006/118/EC) promoted by the European Council aims at preventing and reversing groundwater degradation induced by nitrates due to agricultural practices. This directive requires the member states to identify Nitrate Vulnerable Zones (NVZs), allowing, among other things, for a threshold nitrate concentration value of 50 mg L⁻¹ in the water bodies. There is a vigorous debate in Campania because of the update of the NVZs delimitation resulting from the Regional Council resolution n. 762/2017 and the new regional action plan for nitrates vulnerable areas from agricultural sources (Busico et al., 2019). A one-off Action Plan of 100 million euros is about to start reducing the livestock load to vulnerable areas that, since March 2020, have to be subjected to a spreading limit of 170 kg of nitrogen per hectare per year. Recent studies have reported that over the four-year period of 2012–2015, nitrate concentrations in groundwater reached values higher than the drinking water threshold (50 mg L⁻¹ in Italy), with an increasing trend, in comparison to the previous four-year period (2008–2011) (Ducci et al., 2019).

As also pointed out by Gómez-Hernández and Wen (1994), the main indicators controlling the vulnerability of shallow groundwater are obtained in the present study by simulating the nitrate fate across a 10-m-thick layered soil profile using Hydrus-1D (Mattern and Van-clooster, 2010; Simůnek et al., 2016; Sprenger et al., 2016b; Mokari et al., 2019). The goal is to build plausible scenario-based model simulations to investigate the fate of nitrate, within a stochastic framework, under random-generated Mediterranean climate forcing conditions. Our investigations refer to the Sele River alluvial plain in Campania, a renowned agri-food district for agricultural produce and buffalo dairy products. The probability distributions of three fundamental indicators are assessed to characterize the nitrate transport: i) annual nitrate

leaching, ii) annual root nitrate uptake, iii) vadose zone nitrate transit time. One hundred 20-yr-long simulations were run for each scenario using Hydrus-1D:

- 1) Scenario 1 assumes 195 kg N ha⁻¹ of nitrate fertilizer (urea) applied annually to estimate the probability distributions of annual cumulative nitrate leaching and root nitrate uptake;
- 2) Scenario 2, instead, assumes 195 kg N ha⁻¹ of nitrate fertilizer (urea) applied only once to estimate the nitrate transit time distribution across the soil profile.

2. Materials and methods

2.1. Site description and available data set

The Sele alluvial plain covers an area of about 500 km² that spans around the Sele River near the city of Salerno, located in the region of Campania, southern Italy. The climate is typically Mediterranean, with cold rainy winters and hot dry summers. 68%, 23%, and 8% of the agricultural land of the Sele River Plain is used for crops, fruit orchards, and grazing pastures, respectively (http://www.agricoltura.regione.campania.it/pubblicazioni/territorio_rurale.html).

The predominant crops are vegetables (8065 ha), including fennel, lettuce, sweet pepper, tomatoes, rocket salad, broccoli, cauliflower, green beans, eggplants, cabbage, and several others. Forages cover about 7481 ha, and maize is the predominant forage, subject to irrigation and fertilization practices. Considering the excessive fragmentation of vegetables, we assumed the maize as the predominant land cover in the study's area, and for this reason, we consider maize in model simulations.

The hydrogeology of the Sele Plain belongs to the Pliocene-Quaternary hydrogeological complex with porous aquifers formed by epiclastic deposits of alluvial and coastal plains (De Vita et al., 2018; Tufano et al., 2020). Groundwater fluxes are triggered by a hydraulic gradient of 0.6% in the east-west direction from the mountainous region situated on the eastern border of the study area towards the coastline. The shallow aquifer permeability ranges between 1.6 × 10⁻³ m s⁻¹ and 2.0 × 10⁻³ m s⁻¹, transmissivity spans between 3.0 × 10⁻² m² s⁻¹ and 4.8 × 10⁻² m² s⁻¹, and storage ranges between 0.3 × 10⁻⁴ and 1.5 × 10⁻⁴ (Cassa per il Mezzogiorno, 1983).

Among multiple nitrate sources, crop management based on nitrogen fertilizers (mainly urea and ammonium sulfate) and animal manure spreading represent the primary threat to groundwater quality (Bonfante et al., 2019). The Campania Regional Council has recently provided a new delimitation of nitrate vulnerable zones (NVZs) influenced by agricultural practices. Maps of NVZs (green areas in Fig. 1b) can be downloaded from the geoportal of the Campania region (<https://sit2.regione.campania.it/content/zone-vulnerabili-ai-nitrati> in Italian). To meet this study's aim, we considered a portion of the Sele alluvial plain with available information on depths to the groundwater table (222.72 km²) within the NVZ (Fig. 1d). A geological study based on 11 core drilling lithostratigraphy surveys (<http://www.difesa.suolo.regione.campania.it/content/view/147/>) reports the main characteristics of the geological setting. The vadose zone is characterized by silty-clay alluvial deposits. According to the USDA soil classification, we report a predominance of Mollic HAPLOXERETS, Typic HAPLOXERETS, and Typic CALCIXERETS.

Soil physical and chemical properties, namely percentages of sand (*Sa*), silt (*Si*), and clay (*Cl*), soil oven-dry bulk density (ρ_b), and organic carbon (*OC*), are available from a recent study that was conducted on the farmland in Campania within the *Campania Trasparente* project (Nasta et al., 2020b). Soil samples were collected on the soil surface (topsoil samples) and at soil depths spanning between 80 cm and 110 cm (subsoil samples) to determine soil physical and chemical properties. A total of 3316 and 500 soil samples in the topsoil and subsoil, respectively, were collected in Campania (Nasta et al., 2020a). In the study area of the

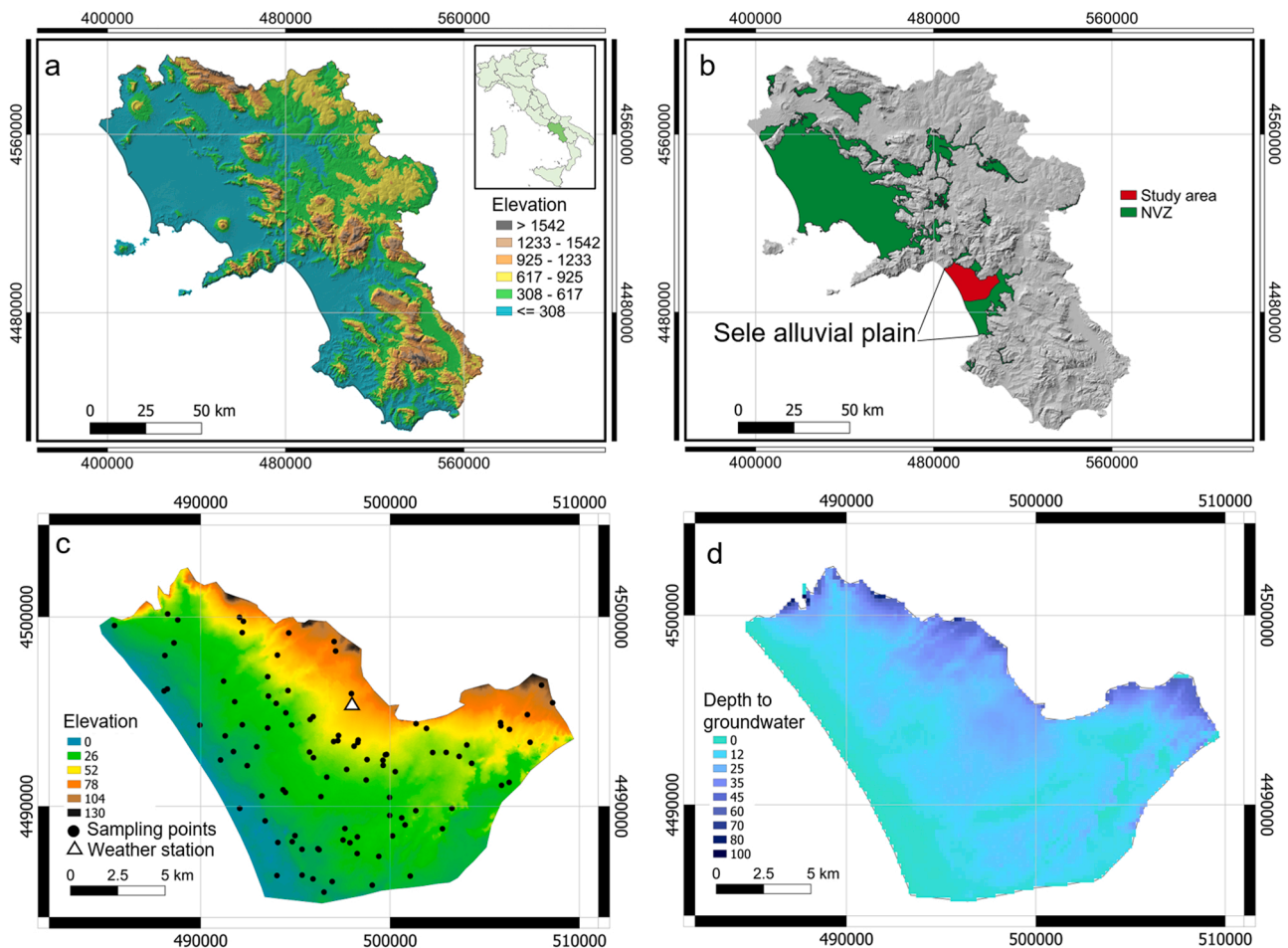


Fig. 1. a) Digital Elevation Model (DEM) of Campania Region, b) nitrate vulnerable zones, NVZs (green area) in Campania (<https://sit2.regione.campania.it/content/zone-vulnerabili-ai-nitrati>) and the study area (red area) in the Sele alluvial Plain, c) DEM of the study area with 86 topsoil samples (black circles), and d) the depth to groundwater in the study area. (For interpretation of the references to color in this figure legend, the reader is referred to the web version of this article.)

Sele alluvial plain, a total of 86 topsoil (representing the uppermost 15 cm of soil profile) and 50 subsoil (in the range from 90 cm to 120 cm soil depths) undisturbed samples were collected (Fig. 1c) (Table 1). These soil samples were used to map the values of sand, silt, and clay content, oven-dry soil bulk density, and soil organic carbon (Fig. S1 in Supplemental Material). The OC values were not measured for the subsoil cores.

A weather station is located near the city of Battipaglia (33 N 497,979 m, 4,495,588 m, 64 m a.s.l.), where daily values of rainfall (*R*)

Table 1

Descriptive statistics for oven-dry bulk density (ρ_b), percentages of sand (*Sa*), silt (*Si*), and clay (*Cl*), and soil organic carbon (*OC*) content for 86 topsoil and 50 subsoil samples in the experimental area in the Sele alluvial Plain (from Nasta et al., 2020b).

		ρ_b g/ cm ³	Sand %	Silt %	Clay %	OC %
Topsoil	Mean	1.37	28.21	38.43	33.36	1.71
	Standard deviation	0.15	10.56	8.94	9.96	1.04
	Coefficient of variation	11.1	37.4	23.3	29.9	61.1
	Minimum	1.08	3.35	18.30	13.22	0.054
	Maximum	1.70	64.10	63.45	60.88	5.59
Subsoil	Mean	1.23	24.86	35.72	39.43	
	Standard deviation	0.20	14.70	10.39	12.98	
	Coefficient of variation	16.1	59.1	29.1	32.9	
	Minimum	0.12	3.00	13.09	8.71	
	Maximum	1.44	78.12	55.45	67.19	

and daily minimum and maximum temperature data are available from 1999 to 2018 (20-yr long time series). In the recording period, the mean annual rainfall is 89.0 cm, and the mean annual temperature is 17.1 °C. Daily values of grass-reference potential evapotranspiration (ET_0) were calculated using the temperature-based method proposed by Hargreaves (Hargreaves and Allen, 2003). This relation only requires the minimum and maximum temperatures, while the extraterrestrial radiation term is estimated using the study site’s latitude and the day of the year. For the Sele River plain, Pelosi et al. (2016) have demonstrated that the Hargreaves equation’s performance proved to be comparable to that of the well-known physically-based Penman-Monteith equation (Allen et al., 1998). The mean annual ET_0 is 111.5 cm. Assuming a uniform land cover of maize (*Zea mays* L.), crop-specific potential evapotranspiration (ET_p) under standard conditions and without water limitations is calculated by multiplying ET_0 by the specific crop (maize) coefficient, K_c (i.e., $ET_p = K_c \times ET_0$). The leaf area index (*LAI*) is used to partition ET_p into potential evaporation (E_p) and potential transpiration (T_p) using the following equation (Ritchie, 1972):

$$E_p = ET_p e^{-0.463LAI} \quad (1)$$

Potential transpiration, T_p (corresponding to potential root water uptake), is obtained by subtracting potential evaporation (Eq.1) from ET_p . The crop coefficient (K_c ; dimensionless), the leaf area index (*LAI*; dimensionless), and the maximum root depth for maize are time-variable and change daily (more details are reported in the Supplementary material) (Nasta and Gates, 2013; Bonfante et al., 2019; Corbari et al., 2021).

By referring to the daily data recorded at the Battipaglia weather station from 1999 to 2018, the annual mean sum of ET_p is 57.6 cm, representing a reduction of about 50% of ET_0 (see Fig. S3 in Supplementary material and Table 2). Annual mean sums of T_p and E_p are 40.4 cm and 17.2 cm, respectively, representing about 70% and 30% of ET_p , respectively.

Rainfall interception (I_R) was calculated using the following formula (Braden, 1985):

$$I_R = aLAI \left(1 - \frac{1}{1 + bP/aLAI} \right) \quad (2)$$

where a (cm d^{-1}) is assumed equal to 0.025 cm d^{-1} and $b = 1 - e^{-0.463LAI}$. Interception is subtracted from measured rainfall to obtain net rainfall (R_{net}). Descriptive statistics of annual mean sums of the aforementioned weather components are reported in Table 2.

Farmers in the Sele River plain mostly apply urea as fertilizer. Urea is incorporated into the soil by rototilling to reduce volatilization. We explored two agricultural practices when urea is applied with a single treatment (195 kg N ha^{-1}) on April 1st or a sequence of three treatments (65 kg N ha^{-1}) on April 1st, June 1st, and August 1st (Bonfante et al., 2019). Heterotrophic bacteria hydrolyze urea ($(\text{NH}_2)_2\text{CO}$) to form ammonium (NH_4^+), which is sequentially nitrified by autotrophic bacteria to nitrite (NO_2^-) and nitrate (NO_3^-) that, in turn, is subsequently denitrified to form dinitrogen (N_2 and N_2O). Since anaerobic conditions rarely occur in the deep vadose zone profile, we neglect the denitrification process (transformation of NO_3^- into N_2 and N_2O) (Hanson et al., 2006; Ramos et al., 2012; Bradshaw et al., 2013; Deb et al., 2016; Busico et al., 2020). Therefore, the following three solute species are considered in this study: $(\text{NH}_2)_2\text{CO} \rightarrow \text{NH}_4^+ \rightarrow \text{NO}_3^-$.

2.2. Soil water balance and nitrate transport simulation with Hydrus-1D

The water balance in the soil-plant-atmosphere system was evaluated using Hydrus-1D (Šimůnek et al., 2016), which numerically solves the one-dimensional Richards equation:

$$\frac{\partial \theta}{\partial t} = \frac{\partial}{\partial z} \left[K(\psi) \left(\frac{\partial \psi}{\partial z} + 1 \right) \right] - \xi(z, \psi, T_p) \quad (3)$$

where t is time, expressed in units of days (d), ψ is the matric pressure head (cm), z is soil depth (positive upward) (cm), θ ($\text{cm}^3 \text{ cm}^{-3}$) is the soil water content, and $\xi(z, \psi, T_p)$ is the sink term (d^{-1}) describing the actual plant root water extraction rate function depending on z , ψ , and potential transpiration (T_p). Hydrus-1D numerically solves the partial-differential Eq. (3) by using a finite element scheme for the spatial discretization and a finite difference scheme for the time discretization. The soil water retention function $\theta(\psi)$ is described by van Genuchten's equation (van Genuchten, 1980):

$$\theta(\psi) = \theta_r + \frac{\theta_s - \theta_r}{[1 + (\alpha|\psi|^n)]^m} \quad (4)$$

where α (cm^{-1}), m (-), and n (-) are water retention shape parameters,

Table 2

Descriptive statistics of annual sums of gross rainfall (R), rainfall interception (I_R), net rainfall (R_{net}), grass-reference potential evapotranspiration (ET_0), maize potential evapotranspiration (ET_p), potential evaporation (E_p), and potential transpiration (T_p).

	R cm	I_R Cm	R_{net} cm	ET_0 cm	ET_p cm	E_p cm	T_p cm
Mean	89.2	1.5	87.5	111.5	57.6	17.2	40.4
Standard deviation	22.1	0.6	21.7	3.5	1.8	0.5	1.3
Coefficient of variation	24.8	37.4	24.8	3.2	3.2	3.2	3.3
Minimum	43.3	0.6	42.1	107.0	55.1	16.6	38.5
Maximum	126.8	2.7	124.2	121.1	62.6	18.8	43.9

and θ_r ($\text{cm}^3 \text{ cm}^{-3}$) and θ_s ($\text{cm}^3 \text{ cm}^{-3}$) are residual and saturated soil water contents, respectively. The two parameters m and n are related as follows: $m = 1 - 1/n$ (van Genuchten, 1980).

Considering the degree of saturation, $S_e = (\theta - \theta_r)/(\theta_s - \theta_r)$, which varies from 0 ($\theta = \theta_r$) to 1 ($\theta = \theta_s$), the unsaturated hydraulic conductivity function, $K(S_e)$ is given by the following equation (van Genuchten, 1980):

$$K(S_e) = K_s S_e^c \left[1 - (1 - S_e^{1/m})^m \right]^2 \quad (5)$$

where K_s (cm d^{-1}) is the saturated hydraulic conductivity and τ (-) is a tortuosity parameter that is assumed to be $\tau = 0.5$ (Mualem, 1976).

Given that the mode of the statistical distribution of depths to the water table is about 10 m within the study area in the Sele alluvial plain (not shown), we set the thickness of the soil profile to be 10 m. The lower boundary condition is set to a constant pressure head ($\psi = 0$ cm), expressing a constant level of the water table of the shallow aquifer. The upper boundary condition depends on fluxes occurring at the soil surface (R_{net} and E_p).

Plant potential transpiration, T_p , determines potential root water uptake (a sink term in the Richards equation) in the soil profile. The root distribution is assumed to be linear in the soil profile by varying from a maximum at the soil surface to a minimum at the maximum rooting depth, which is considered time-variant (see Fig. 3c). Both E_p and T_p are reduced by water limitation and stresses to actual evaporation (E_a) and actual transpiration (T_a). The actual root water extraction rate, ξ , is modeled using the method proposed by Feddes et al. (1978). Maize T_p is reduced between $\psi = -500$ cm and the wilting point that corresponds to $\psi_{wp} = -8000$ cm. To mitigate excessive root water uptake stress of maize during the dry growing season, Hydrus-1D has an option to trigger irrigation when a user-specified pressure head is reached in a selected observation node. Irrigation starts after a user-specified lag period at a user-specified irrigation rate. The duration of irrigation is also specified.

When surficial matric pressure head, ψ_{surf} , is less than a threshold value, ψ_{min} , the prescribed flux boundary condition (a Neumann condition) specified at the upper boundary of the soil profile automatically switches to a constant pressure head boundary condition (a Dirichlet condition), resulting in a reduction of potential evaporation (E_p) into actual evaporation (E_a). A proportion of net rainfall, R_{net} , is turned into runoff when ψ_{surf} exceeds the maximum soil surface matric potential value, ψ_{max} , that represents the nominal depth of surface water ponding allowable before runoff generation.

Hydrus-1D simultaneously considers the fate and transport of multiple solutes subjected to first-order degradation reactions. Hanson et al. (2006) considered a urea-ammonium-nitrate fertigation system subject to nitrogen (N) transformation processes. Urea, $(\text{NH}_2)_2\text{CO}$, degrades to ammonium, NH_4^+ , that is subsequently transformed into nitrate, NO_3^- , by the process of nitrification. NO_3^- is then subject to denitrification. The partial differential equations governing the one-dimensional transport of N involved in sequential first-order decay chain reactions during transient water flow in a variably-saturated rigid porous medium are taken as:

$$\frac{\partial \theta C_1}{\partial t} = \frac{\partial}{\partial z} \left(\theta D_1^w \frac{\partial C_1}{\partial z} \right) - \frac{\partial q C_1}{\partial z} - \mu'_{w,1} \theta C_1 \quad (6)$$

$$\frac{\partial \theta C_2}{\partial t} + \frac{\partial \rho_b S_2}{\partial t} + \frac{\partial a_v g_2}{\partial t} = \frac{\partial}{\partial z} \left(\theta D_2^w \frac{\partial C_2}{\partial z} \right) + \frac{\partial}{\partial z} \left(a_v D_2^g \frac{\partial g_2}{\partial z} \right) - \frac{\partial q C_2}{\partial z} - \mu'_{w,2} \theta C_2 + \mu'_{w,1} \theta C_1 - r_{a,2} \quad (7)$$

$$\frac{\partial \theta C_3}{\partial t} = \frac{\partial}{\partial z} \left(\theta D_3^w \frac{\partial C_3}{\partial z} \right) - \frac{\partial q C_3}{\partial z} - \mu_{w,3} \theta C_3 + \mu'_{w,2} \theta C_2 - r_{a,3} \quad (8)$$

where C is the solute concentration in the liquid phase (mg L^{-1}), S is the solute concentration in the solid phase (mg g^{-1}), g is the solute concentration in the gas phase (mg L^{-1}), θ is the volumetric water content (cm^3

cm^{-3}), ρ_b is the oven-dry bulk density (g cm^{-3}), a_v is the air content ($\text{cm}^3 \text{cm}^{-3}$), q is the volumetric flux density (cm d^{-1}), μ_w is the first-order rate constant for the solute in the liquid phase (d^{-1}), μ'_w is the first-order rate constant providing the connection between individual nitrogen species in the liquid phase (d^{-1}), r_a is the root nutrient uptake term ($\text{mg L}^{-1} \text{d}^{-1}$), D^w is the dispersion coefficient ($\text{cm}^2 \text{d}^{-1}$) for the liquid phase, and D^g is the diffusion coefficient ($\text{cm}^2 \text{d}^{-1}$) for the gas phase. The subscripts 1, 2, and 3 represent $(\text{NH}_2)_2\text{CO}$, NH_4^+ , and NO_3^- , respectively.

The dispersion coefficient in the liquid phase, D^w , is given as:

$$D^w = D_L \frac{|q|}{\theta} + D_w \tau_w \quad (9)$$

where D_w is the molecular diffusion coefficient in free water ($\text{cm}^2 \text{d}^{-1}$), τ_w is a unitless tortuosity factor in the liquid phase, $|q|$ is the absolute value of the Darcian fluid flux density (cm d^{-1}), and D_L is the longitudinal dispersivity (cm).

2.3. Set-up of Hydrus-1D for the Sele alluvial plain

According to Nasta et al. (2020a), rainfall variability was quantified with synthetic rainfall time series considering an alternation of two 6-month lasting seasons (see Fig. S4 in Supplementary material). A wet season includes the months of October, November, December, January, February, and March (when the sum of monthly average R is higher than the sum of monthly average ET_p) while the remaining months define the dry season (i.e., from April to September). In each of these two seasons, rainfall is modeled by a stochastic Poisson point process, with daily rainfall depth μ (cm) and occurrence λ (d^{-1}). A total of one hundred synthetic rainfall time series of 7304 daily values (corresponding to 20 years) were generated, keeping constant parameters of the Poisson process and daily rainfall parent distribution in each season. In each modeling scenario, the synthetic time series was then used as input for the Hydrus-1D to evaluate the effects of rainfall seasonality on the water balance components. The Poisson parameters calculated from the daily rainfall values (1999–2018) measured at the Battipaglia weather station are $\mu = 0.88$ cm and $\lambda = 0.39 \text{ d}^{-1}$ for the wet season and $\mu = 0.67$ cm and $\lambda = 0.21 \text{ d}^{-1}$ for the dry season.

Table 3 reports basic statistics of ET_p components available from 1999 to 2018 at the Battipaglia weather station. A total of one hundred synthetic E_p and T_p time series of 7304 daily values (corresponding to 20 years) were then generated using random numbers drawn from a normal distribution with a mean and standard deviation in each month of the year reported in Table 3.

A similar-media scaling method was used in this study to characterize the soil hydraulic behavior of the study area. This scaling approach is conceptualized by replacing the heterogeneous porous domain with a homogeneous soil domain when assuming the validity of

Table 3

Descriptive statistics in terms of monthly mean and standard deviation of daily values of potential evaporation, E_p , potential transpiration, T_p , calculated from 20-yr long daily temperature data at the Battipaglia weather station.

Month	E_p (cm d^{-1})		T_p (cm d^{-1})	
	Mean	Standard deviation	Mean	Standard deviation
Jan	0.022	0.004	0	0
Feb	0.031	0.005	0	0
Mar	0.046	0.009	0	0
Apr	0.066	0.011	0	0
May	0.082	0.015	0.031	0.034
Jun	0.080	0.013	0.250	0.091
Jul	0.048	0.007	0.484	0.070
Aug	0.052	0.009	0.391	0.073
Sep	0.053	0.007	0.140	0.048
Oct	0.037	0.007	0.019	0.015
Nov	0.029	0.005	0	0
Dec	0.020	0.004	0	0

the Miller-Miller geometric similarity hypothesis (Miller and Miller, 1956; Clausnitzer et al., 1992). In other words, the sparse point-scale soil hydraulic functions over the heterogeneous spatial domain coalesce into a single reference soil hydraulic function (a reference water retention function, WRF_{ref} , and a reference hydraulic conductivity function, HCF_{ref}), referring to a homogeneous spatially representative soil domain through a set of scaling factors (Nasta et al., 2013).

A representative soil profile was set with two functional soil layers (a topsoil layer from the soil surface to the depth of 100 cm overlying a subsoil layer between soil depths of 100 cm and 1000 cm) according to measurement depths described beforehand. The five unknown soil hydraulic parameters (α , n , θ_r , θ_s , and K_s) describing the soil water retention and hydraulic conductivity functions for each of the two soil layers have been estimated in the study area by combining the HYPRES pedotransfer function (PTF) (Wösten et al., 1999) with the Miller-Miller geometric similarity theory (Clausnitzer et al., 1992). Gridded values (2 km grid size) of sand, silt, and clay, oven-dry soil bulk density, and soil organic carbon have been used as input of the HYPRES-PTF to retrieve the soil hydraulic properties of both topsoil and subsoil layers, whereas parameter θ_r was set at zero. More details are presented in Supplemental Materials (Fig. S5), and Table 4 reports the soil hydraulic parameters attributed to topsoil and subsoil in the representative soil profile.

Initial conditions in the soil profile were set as the soil water content values at field capacity, which is a reasonable condition on January 1st, in the wet season. Some farmers were interviewed to investigate their irrigation management and the factors influencing the irrigation schedule, the irrigation water volume, and the duration of each irrigation event. The irrigation schedule is based on farmers' experience in detecting soil dryness. It is impossible to quantify the exact amount of irrigation water, and many farmers stop irrigation when infiltration decreases or water ponds are noticed. The irrigation events start at the soil pressure head corresponding to field capacity and end at the soil pressure head at the maize initial root water stress (Romano and Santini, 2002). Therefore, to mimic farmers' behavior as close as possible, irrigation was triggered with zero lag time when the pressure head at the soil depth of 0.60 m (the depth of a tensiometer and a corresponding control node in Hydrus-1D) reaches ψ at field capacity (ψ_{FC}) (Bonfante et al., 2019), given by the following physically-based analytical equation proposed by Assouline and Or (2014):

$$|\Psi_{\text{FC}}| = \frac{1}{\alpha} \left(\frac{n-1}{n} \right)^{(1-2n)/n} \quad (10)$$

To calculate the effective soil hydraulic parameters in the representative soil profile, the parametric aggregation approach presented in Nasta and Romano (2016) was employed by obtaining $\psi_{\text{FC}} = -207$ cm. The irrigation rate was set to 1.0 cm d^{-1} , and the irrigation duration to 1 day.

Urea and nitrate are assumed to be present only in the dissolved phase (the distribution coefficient, $K_d = 0 \text{ cm}^3 \text{g}^{-1}$), ammonium was assumed to adsorb to the solid phase by setting $K_d = 3.5 \text{ cm}^3 \text{g}^{-1}$ (Hanson et al., 2006). The first-order decay coefficients μ'_w for urea (hydrolysis) and ammonium (nitrification) were set to 0.38 d^{-1} and 0.2 d^{-1} ,

Table 4

Soil hydraulic parameters for the reference WRF_{ref} and HCF_{ref} of the topsoil and subsoil in the soil profile.

	Parameter	Unit	
Topsoil	θ_s	$\text{cm}^3 \text{cm}^{-3}$	0.447
	α	cm^{-1}	0.0348
	n	–	1.34
	K_s	cm d^{-1}	24.87
Subsoil	θ_s	$\text{cm}^3 \text{cm}^{-3}$	0.602
	α	cm^{-1}	0.0231
	n	–	1.29
	K_s	cm d^{-1}	13.16

respectively. Li et al. (2015) recommended that the molecular diffusion coefficients in free water (D_w) for NH_4^+ and NO_3^- were 1.52 and 1.64 $\text{cm}^2 \text{d}^{-1}$, respectively. We assumed $D_w = 1.52 \text{ cm}^2 \text{d}^{-1}$ also for urea. The longitudinal dispersivity was assumed to be 10 cm (1/10th of the surface layer). The tortuosity factor in the liquid phase, τ_w , is calculated using the relationship proposed by Millington and Quirk (1961). Unlimited passive uptake of both NH_4^+ and NO_3^- was allowed in the root solute uptake model (Simunek and Hopmans, 2009) by specifying the maximum allowed uptake concentration exceeding NO_3^- concentrations recorded in the root zone.

Fertilization is given in the form of urea (solute 1), and a total annual amount of 195 $\text{kg N ha}^{-1} \text{y}^{-1}$ is applied on the soil surface (Bonfante et al., 2019) in two different agricultural practices:

- 1) In a single treatment on April 1st (agricultural practice#1);
- 2) In a sequence of three treatments (65 kg N ha^{-1}) on April 1st, June 1st, and August 1st (agricultural practice#2).

Fertilization in Hydrus-1D depends on the time-dependent water flux (precipitation) and concentration (called “ c_{Top} ”) at the soil surface boundary. We imposed $R_{\text{net}} (= 1.0 \text{ cm} > E_p)$ to ensure solute entering the soil profile. For example, the amount of 195 kg N ha^{-1} corresponds to a solute mass per unit area of $S = 0.00195 \text{ g cm}^{-2}$. Therefore, by specifying the water depth, $L = R_{\text{net}} = 1.0 \text{ cm}$, the nitrate concentration in water is $c_{\text{Top}} = S/L = 0.00195 \text{ g cm}^{-3}$ (1950 mg L^{-1}).

2.4. Scenario 1: assessment of root nitrate uptake and nitrate leaching

In Scenario 1, realistic agricultural management is mimicked when the total annual amount (195 kg N ha^{-1}) of urea, $(\text{NH}_2)_2\text{CO}$, is applied every year for 20 years, starting from the first year. One set of one hundred model simulations was considered when the total amount of urea is applied with a single annual treatment (agricultural practice#1) on April 1st, and another set of one hundred model simulations was considered when the total amount of urea is applied in three treatments (agricultural practice#2) on April 1st, June 1st, and August 1st (Fig. 2). Daily R , E_p , and T_p data were stochastically generated over 20 years to ensure the impact of the Mediterranean seasonal climate regime on the water balance. This exercise obtains probability distributions of annual cumulative nitrate flux at the soil profile bottom and root nitrate uptake. A Matlab script was used to automatically change daily R , E_p , and T_p values in the input text file “ATMOSPH.IN” and extract results on nitrate from the output text files “solute3.out” and “Obs_Node.out”.

2.5. Scenario 2: assessment of nitrate transit time

In Scenario 2, the transit time is defined as the time required for a solute (in this case urea, solute 1) applied on a single day of a single

specific year at the soil surface to transform (into nitrate, solute 3) and migrate to the soil profile bottom by entering the shallow aquifer (Fig. 3). The transit time corresponds to the difference between the peak of the nitrate breakthrough curve (BTC) at the soil profile bottom and fertilizer application date. In the case of a single treatment (agricultural practice#1), one fertilizer application is set with 1.95 mg cm^{-3} of urea, $(\text{NH}_2)_2\text{CO}$ (corresponding to 195 kg N ha^{-1}), applied at the soil surface on April 1st only in the third year. In the case of three-treatment applications (agricultural practice#2), instead, three individual sets of model simulations in the third year were organized. The third year (instead of the first year) was selected to minimize the impact of unknown initial conditions (the first two years of simulation thus represent a warm-up period). As mentioned above, daily R , E_p , and T_p data were stochastically generated over 20 years. This exercise was repeated one hundred times to obtain a transit time distribution (TTD). As above, a Matlab script was used to provide model inputs and extract model results automatically.

3. Results

3.1. Results for Scenario 1: assessment of root nitrate uptake and nitrate leaching

A Monte Carlo analysis is performed with randomly generated boundary fluxes to determine the probability distributions of annual cumulative root nitrate uptake and nitrate leaching when fertilizer is applied every year. Recall that new synthetic time-series of daily precipitation and crop-specific potential evapotranspiration data were stochastically generated by considering the typical climate seasonality under Mediterranean conditions.

One hundred simulated time series of daily root nitrate uptake and nitrate leaching under agricultural practice#1 and agricultural practice#2 are illustrated in Fig. 4. In general, root nitrate uptake depends on the timing and amount of fertilization, time-variant maize characteristics, and water balance, which is influenced by precipitation, crop-specific potential evapotranspiration, and irrigation. Crop-specific potential evapotranspiration depends on the time-variant crop coefficient that is maximum ($K_c = 1.05$) for a short period from July 16th (DOY 197) to August 2nd (DOY 214) during tassel, silking, and blister-kernel phases (Fig. S2). July’s highest crop coefficient value induces maximum crop-specific potential evapotranspiration equal to 0.532 cm d^{-1} (Table 3). During the dry season, soil water deficit causes a reduction of potential transpiration into actual transpiration.

Irrigation mitigates soil water deficit during the dry season and helps reduce root water stress by increasing actual transpiration fluxes and consequently root nitrate uptake. Indeed, while annual mean potential transpiration is 40.4 cm (Table 2), annual mean actual transpiration simulated in Hydrus-1D is 32.5 cm (about a 20% reduction of T_p into

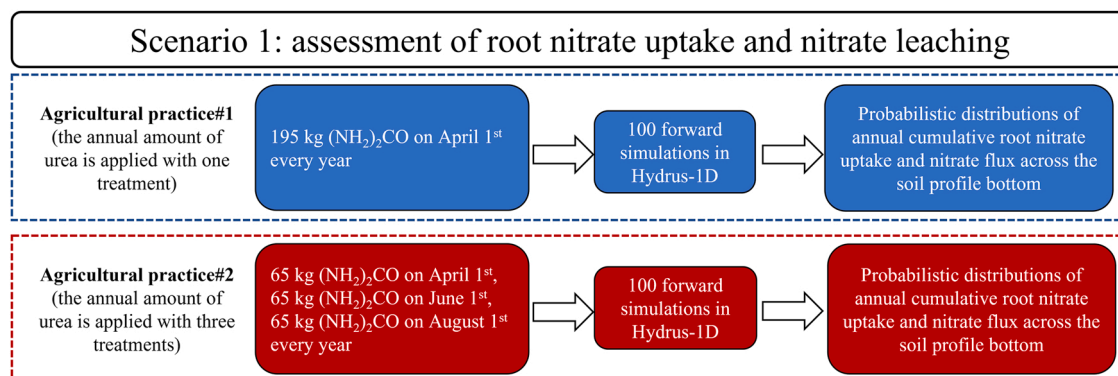


Fig. 2. Schematic overview of Scenario 1: single and multiple treatments of fertilizer are applied every year to assess probability distributions of root nitrate uptake and nitrate leaching.

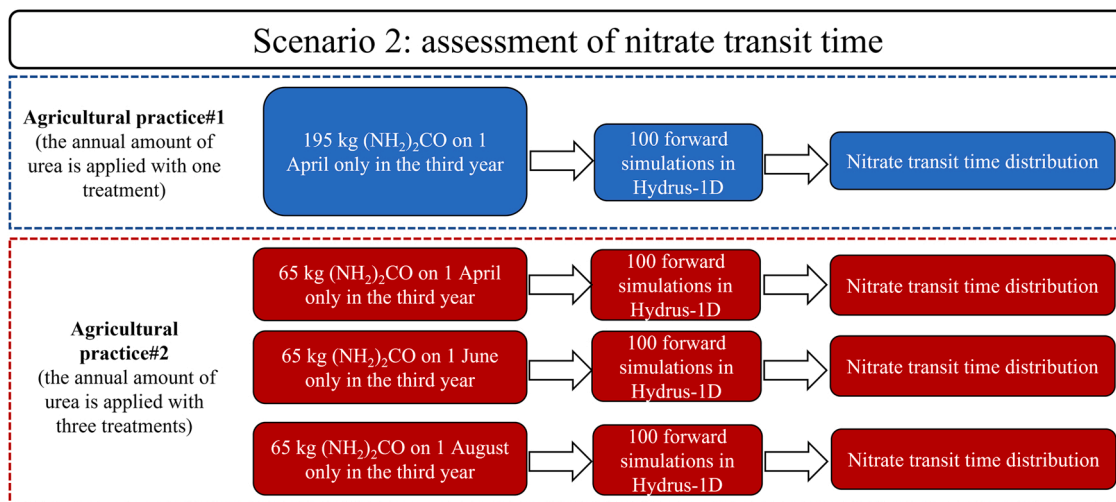


Fig. 3. Schematic overview of Scenario 2 for assessing probability distributions of nitrate transit time.

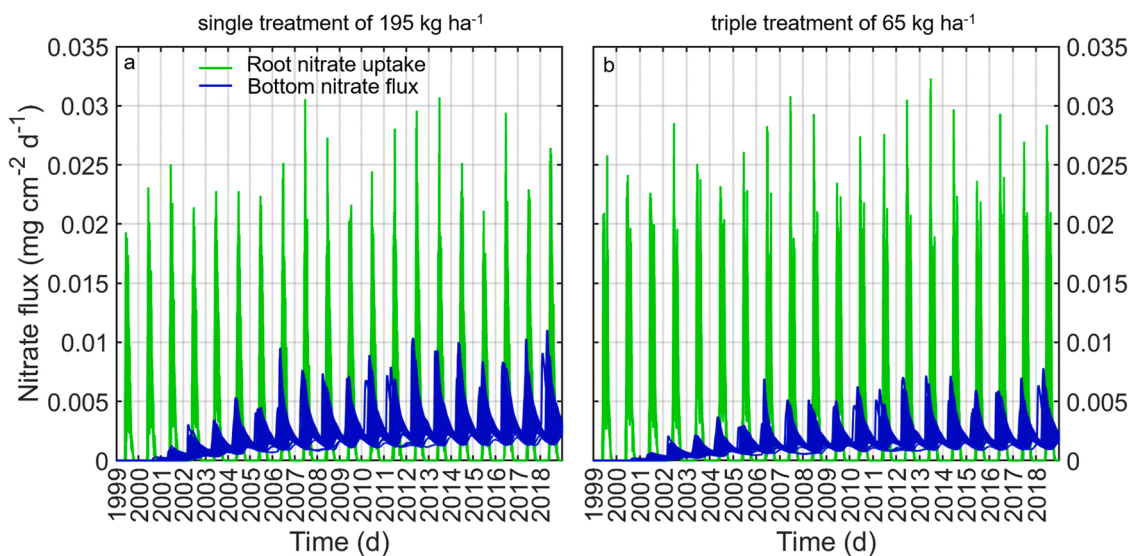


Fig. 4. Simulated root nitrate uptake (green line) and nitrate leaching (blue line) obtained using one hundred simulations considering fertilization with a) one treatment (195 kg N ha^{-1}) on April 1st every year, and b) three treatments (65 kg N ha^{-1}) on April 1st, June 1st, and August 1st every year. (For interpretation of the references to color in this figure legend, the reader is referred to the web version of this article.)

T_a). Annual cumulative irrigation simulated in Hydrus-1D is between 36.9 cm (corresponding to 3685 m^3 per hectare) and 40.7 cm (corresponding to 4065 m^3 per hectare) with an average amount of 38.2 cm (corresponding to 3819 m^3 per hectare). While this amount seems plausible, some farmers might irrigate using even 50% more water (http://www.agricoltura.regione.campania.it/irrigazione/prci_risultati.html). Bonfante et al. (2019) estimated total irrigation amounts on average between $2819 \text{ m}^3 \text{ ha}^{-1}$ and $4699 \text{ m}^3 \text{ ha}^{-1}$. Under Mediterranean semiarid climate conditions in northeast Spain, farmers apply on average 81.8–86.2 cm of irrigation water for maize, considering annual mean precipitation of 34.7–44.3 cm and grass-reference evapotranspiration of 123.0–133.1 cm (Malik et al., 2019).

Nonetheless, in this study, the difference in root nitrate uptake between the two agricultural practices is caused solely by the timing and amount of fertilization since the water balance is the same under both agricultural practices. In agricultural practice#1 (195 kg N ha^{-1} applied on April 1st), the applied nitrate easily bypasses the root zone because roots start growing on May 9th (DOY = 129, Fig. S2). In contrast, in agricultural practice#2 (namely the 3-steps application), nitrate derived from fertilizer applications on June 1st and August 1st is mostly taken up

by roots. Root nitrate uptake increases linearly as a function of time (Eq. S3), with a concurrent increase in potential evapotranspiration (Fig. S3). Moreover, the LAI reaches its maximum value (LAI = 5.5) between July 16th (DOY 197) and August 2nd (DOY 214) (Fig. S2), maximizing potential root water uptake and minimizing potential evaporation from the soil surface (Fig. 5a). Actual transpiration reaches its maximum value at the beginning of the mature growth phase, with favorable climate conditions from middle August (Fig. 5a). This interpretation highlights the importance of adequately describing various stages of the maize growing season, which are well-documented (Nasta and Gates, 2013; Bonfante et al., 2019). Fig. 5b shows median daily root nitrate uptake values under agricultural practice#1 (red line) and agricultural practice#2 (blue line) during the year, with distinct maize growth phases.

The total nitrate removed by roots during crop planting, emergence (CPE), tassel, silking, and blister-kernel phases (BK) is 0.589 mg cm^{-2} ($58.9 \text{ kg N ha}^{-1}$) and 0.648 mg cm^{-2} ($64.8 \text{ kg N ha}^{-1}$) under agricultural practice#1 and agricultural practice#2, respectively. In contrast, the main difference in root nitrate uptake is observed during the mature growth phase (MG), with 0.213 mg cm^{-2} ($21.3 \text{ kg N ha}^{-1}$) removed under agricultural practice#1 and 0.476 mg cm^{-2} ($47.6 \text{ kg N ha}^{-1}$)

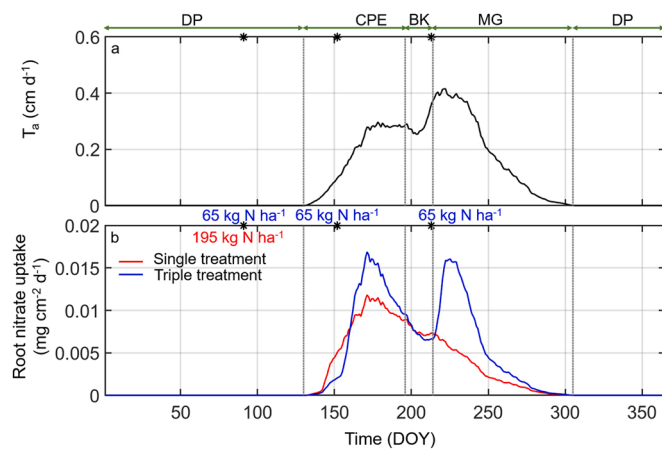


Fig. 5. Daily median values of simulated a) actual transpiration, T_a , and b) root nitrate uptake considering single (red line) and triple (blue line) application treatments. The black asterisks indicate fertilizer applications on April 1st, June 1st, and August 1st. Vertical gray dotted lines delimit a dormant period (DP), maize planting and emergence (CPE), tassel, silking, and blister-kernel phases (BK), and mature growth phase (MG). (For interpretation of the references to color in this figure legend, the reader is referred to the web version of this article.)

removed under agricultural practice#2. In the latter case, the third treatment applied on August 1st (third black asterisk on DOY 213 in Fig. 5) boosts root nitrate uptake (blue line in Fig. 5b) during the mature growth phase. The impact of harvest timing (usually from middle September to middle October) on root nitrate uptake is negligible under both agricultural practices.

Fig. 6 shows the frequency distribution of annual cumulative root solute uptake and nitrate leaching based on one hundred forward simulations. Two normality tests (Lilliefors and Kolmogorov-Smirnov executed in Matlab) reject the null hypothesis that both annual cumulative root solute uptake and nitrate leaching (under both agricultural practices) come from a normal distribution at the 5% significance level.

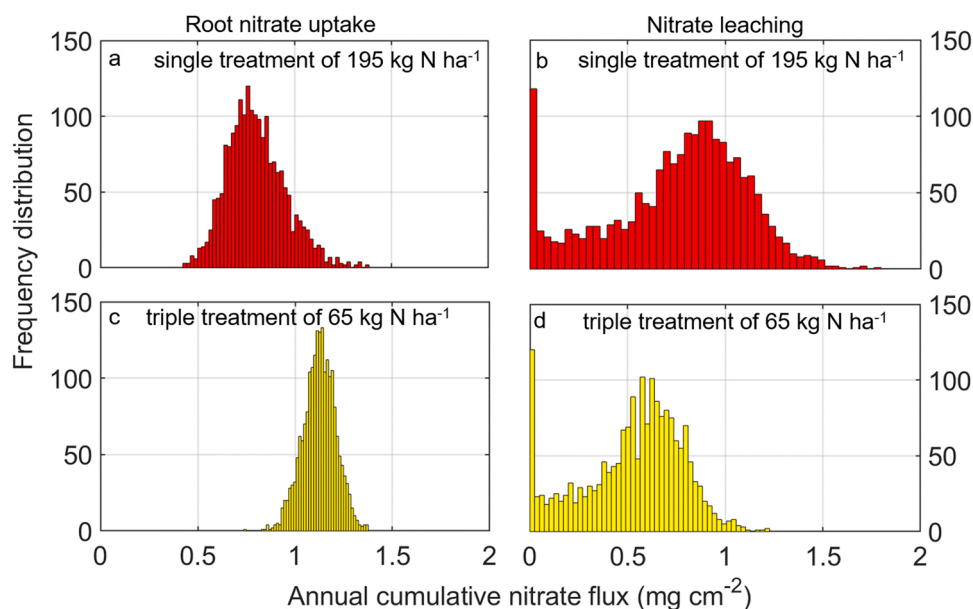


Fig. 6. Frequency distribution of 20 annual cumulative nitrate fluxes in one hundred forward modeling simulations: a) root nitrate uptake in agricultural practice#1; b) nitrate leaching in agricultural practice#1; c) root nitrate uptake in agricultural practice#2; d) nitrate leaching in agricultural practice#2.

Therefore, the median is presented instead of the mean as a representative value of each frequency distribution. The zero is the most frequent value (mode) in annual cumulative nitrate leaching (Fig. 6b and d) because the nitrate flux across the soil profile bottom remains zero during the first two years of the numerical simulations. The one-treatment fertilization (see red histograms in Fig. 6a and b) results in a median value of annual cumulative root nitrate uptake of 0.803 mg cm^{-2} (corresponding to $80.3 \text{ kg N ha}^{-1}$) and annual cumulative nitrate leaching of 0.749 mg cm^{-2} (corresponding to $74.9 \text{ kg N ha}^{-1}$). In other words, roots absorb 41% of applied nitrate, while median annual cumulative nitrate leaching represents about 38% of applied nitrate. The three-treatment fertilization (see yellow histograms in Fig. 6c and d) results in a median value of annual cumulative root nitrate uptake of 1.12 mg cm^{-2} (corresponding to 112 kg N ha^{-1}) and annual cumulative nitrate leaching of 0.524 mg cm^{-2} (corresponding to $52.4 \text{ kg N ha}^{-1}$). Almost 60% of applied nitrate is removed by root nitrate uptake, while median annual cumulative nitrate leaching represents about 27% of applied nitrate. Considering the total amount of fertilizer applied during 20 years is $3900 \text{ kg N ha}^{-1}$, the final amount of residual nitrate in the entire 10-m-thick soil profile after 20 years is on average 796 kg N ha^{-1} (20.4% of applied nitrate) and 612 kg N ha^{-1} (15.7% of applied nitrate) for agricultural practice#1 and #2, respectively. Similarly, cumulative nitrate leaching after 20 years is on average $1498 \text{ kg N ha}^{-1}$ and $1048 \text{ kg N ha}^{-1}$ for agricultural practices #1 and #2, respectively.

In the Po River plain (Lombardy, northern Italy), under annual rainfall conditions fairly similar to those recorded in our study area, Perego et al. (2012) reported for maize fields at six experimental sites an annual irrigation supply ranging between $1800 \text{ m}^3 \text{ ha}^{-1}$ and $3150 \text{ m}^3 \text{ ha}^{-1}$. Annual fertilization amounts were between 309 kg N ha^{-1} and 642 kg N ha^{-1} , plant nitrogen removal between 194 kg N ha^{-1} (57% of the fertilization amount) and 305 kg N ha^{-1} (47%), and nitrate leaching below the root zone ($z = 1.5 \text{ m}$) measured by suction cups ranging between 14 kg N ha^{-1} (4%) and 321 kg N ha^{-1} (50%). Demurtas et al. (2016) reported annual mean precipitation of 56.8 cm , irrigation of $4600 \text{ m}^3 \text{ ha}^{-1}$, mean annual fertilization of 599 kg N ha^{-1} , root nitrate uptake of 264 kg N ha^{-1} (47% of applied nitrate), nitrate leaching of 84 kg N ha^{-1} (15% of applied nitrate), and 250 kg N ha^{-1} residual nitrate (39% of applied nitrate) under Mediterranean climate conditions.

3.2. Results for Scenario 2: assessment of nitrate transit time

A Monte Carlo analysis was performed by generating upper boundary fluxes to determine a probabilistic distribution of nitrate transit time values (TTD). Scenario #2 involves an ensemble of one hundred numerical simulations with Hydrus-1D subjected to daily rainfall data generated by the Poisson distribution parameters pertaining to the dry and wet seasons, and E_p and T_p data with normally distributed parameters (mean and standard deviation) in each month. Once again, recall that the fertilizer is applied only in the third year, either with a single treatment (agricultural practice #1) or with a three-step treatment (agricultural practice #2).

Fig. 7 refers to agricultural practice #1 (i.e., a single treatment of urea) and depicts the ensemble of one hundred nitrate concentrations at soil depths of 300 cm, 600 cm, and 1000 cm (Fig. 7a) and corresponding normal distributions of transit time values (Fig. 7b). These graphs show that nitrate concentration gradually propagates downward through the vadose zone, with BTCs characterized by decreasing magnitude and increasing duration with depth (Fig. 7a). It is hypothesized that below the root zone ($z = 300$ cm, blue lines), the nitrate BTC peaks depend on the combination of daily R_{net} and ET_p following the nitrate spill. The BTCs are affected by water infiltration induced by rainfall, mainly occurring in the wet season. To test this hypothesis, the Pearson's correlation coefficients between the cumulated rainfall and transit time values at the soil depths of 300 cm, 600 cm, and 1000 cm were -0.80 , -0.85 , -0.85 , respectively. This indicates that the TTD values depend highly on R_{net} , accelerating or slowing down nitrate transport through the unsaturated zone. The standard deviation of TTDs increases with soil depth (65.4 days, 145.3 days, and 181.4 days at the soil depths of 300 cm, 600 cm, and 1000 cm, respectively).

When considering agricultural practice #2 (i.e., three applications of urea), Fig. 8 shows the normal probability distributions of the ensemble of one hundred nitrate concentrations at soil depths of 300 cm, 600 cm, and 1000 cm. In general, transit times decrease when treatment is individually applied on April 1st, June 1st, and August 1st. The transit times relevant to the treatment applied in April are very similar to those presented previously and associated with a single treatment of 195 kg N ha^{-1} . For the treatments applied on June 1st and August 1st, the mean transit times are 2707 days (with a standard deviation of 186 days) and 2650 days (with a standard deviation of 185 days), respectively.

It is important to point out that, in the present study, TTDs are affected only by the upper boundary forcing, while other factors were kept fixed, namely i) the soil hydraulic parameters in the two functional soil layers (influencing flow velocity across the unsaturated zone), and ii) the reaction and transport parameters, especially the nitrate

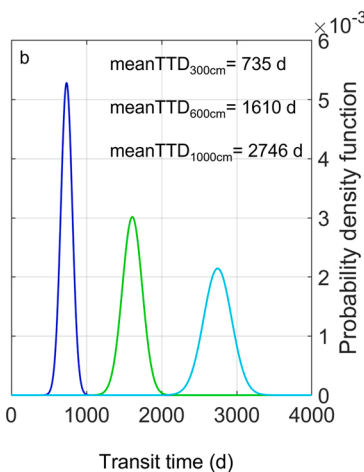
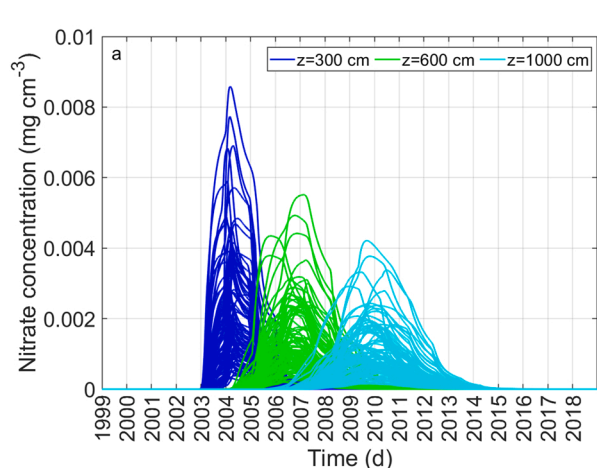


Fig. 7. a) Simulated concentrations at $z = 300$ cm (blue line), $z = 600$ cm (green line), and $z = 1000$ cm (cyan line) by using one hundred simulations when considering one treatment (195 kg N ha^{-1}) on April 1st in the third year and b) probability density function (pdf) of transit times obtained by running one hundred simulations at $z = 300$ cm (blue line), $z = 600$ cm (green line), and $z = 1000$ cm (cyan line). Mean values of transit time distributions (TTD) are reported. (For interpretation of the references to color in this figure legend, the reader is referred to the web version of this article.)

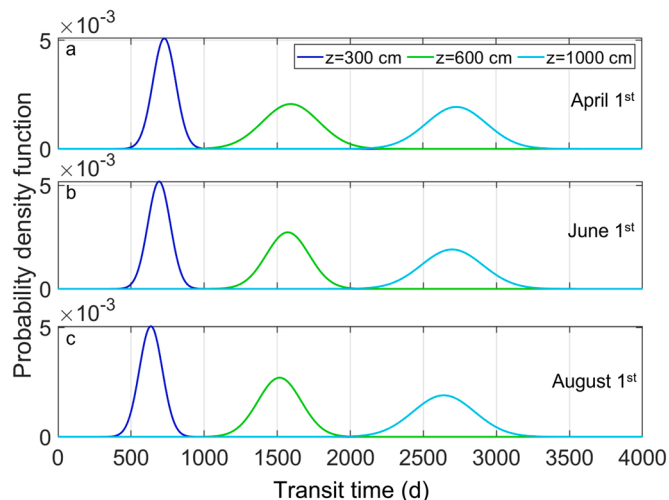


Fig. 8. Probability density function (pdf) of transit times obtained by running one hundred simulations at $z = 300$ cm (blue line), $z = 600$ cm (green line), and $z = 1000$ cm (cyan line) when the treatment is individually applied on a) April 1st, b) June 1st, c) August 1st. (For interpretation of the references to color in this figure legend, the reader is referred to the web version of this article.)

longitudinal dispersivity (affecting the solute transport process).

4. Discussion

In the present study, the nitrate fate was evaluated in a representative 10-m-thick soil profile by using a process-oriented hydrological model supported by a relatively large number of soil data (Nasta et al., 2020b) as well as parameter values describing the nitrogen transport and transformation taken from the literature (Veizaga et al., 2016). However, because of a lack of direct local measurements on nitrate data, our one-dimensional numerical results should not be strictly considered for actual agronomic applications. Indeed, our model simulations provide useful indications of nitrate transport in the area and, more importantly, can be integrated with map overlay procedures for delineating nitrate vulnerable zones (Matzeu et al., 2017; Catani et al., 2020; Vigliotti et al., 2020; Tufano et al., 2020). The method presented in this study identifies process-oriented indicators accounting for the local climatic and environmental conditions. This is, therefore, more effective and understandable to landowners and stakeholders. To our knowledge, this study provides a novel protocol to assess TTDs characterizing nitrate transport within the soil profile to support the mapping of NVZs (Fusco

et al., 2020). If model simulations are assumed valid, the nitrate transit time can be viewed as a “dynamic” indicator of groundwater vulnerability and an efficient way to evaluate the protective function exerted by the vadose zone (Matteau et al., 2019; Turkeltaub et al., 2020).

Quantification of nitrate fate and transport in the vadose zone depends on several factors that may significantly affect the accuracy of the estimated nitrate transit time (Mattern and Vancloster, 2010). Water flow depends on the depth to the groundwater table, soil hydraulic properties of the vadose zone, and maize characteristics influencing evapotranspiration fluxes. Nitrogen species fate and transport depend on their transport and reaction parameters, initial concentrations throughout the soil profile, and the amount and frequency of fertilizer applications.

It is very difficult to characterize soil layering and its soil hydraulic properties throughout large-scale domains. In this study, only information on soil physical properties within the topmost meter of the vadose zone was used to artificially build two functional soil layers over a 10-m-thick soil profile. HYPRES-PTF was employed in each soil layer to retrieve five unknown soil hydraulic parameters (α , n , θ_r , θ_s , and K_s) describing the soil water retention and hydraulic conductivity functions. Other existing PTFs developed on European datasets could be tested as well (Weynants et al., 2009; Szabó et al., 2021; Nasta et al., 2021). The eleven lithological core drilling soil profiles evidence relatively uniform soil physical properties in the vadose zone. Nevertheless, the impact of soil vertical variability on the decay of saturated hydraulic conductivity induced by soil compaction in the deepest soil layers is expected (Turkeltaub et al., 2021). The scenario-based simulations are not supported by monitoring key state variables (water contents, pressure head data) or water fluxes throughout the soil profile. The cost of the instrumentation might be high and unfeasible. Farmers do not recommend the installation of sensors beneath the maize fields because of tillage operations. Some studies interestingly calibrate physical models using soft data approaches such as isotope-based techniques (Stumpp et al., 2012; Sacchi et al., 2013; Sprenger et al., 2016a; Boumaiza et al., 2021).

Future improvements will integrate key measurements of nitrate absorbed by roots, nitrate leaching into the shallow aquifer, and nitrate concentrations measured throughout the soil profile based on stable isotope data. In a subsequent study, farmers’ collaboration will be requested to record the exact amount and frequency of fertilization, fertilizer type, and irrigation depths during the growing season. Our results produce annual root nitrate uptake comparable to previous studies in cornfields (Tafteh and Sepaskhah, 2012).

In a subsequent step, the available gridded soil hydraulic properties will be used in the Hydrus-1D package by assuming the spatial domain represented by independent columns. Hydrus-1D will be coupled to MODFLOW (Beegum et al., 2018, 2019) to describe the nitrate transport influenced by topography and depth to the water table in the 3D domain (Prudic et al., 2004; Zeng et al., 2019).

Another future study will investigate the impact of point source pollution caused by livestock farming (Piccini et al., 2016). The contribution of localized applications of high amounts of buffalo manure on nitrate mineralization will be assessed. In this regard, a refinement of available models is needed to consider the process of nitrate immobilization into the microbial biomass that commonly occurs for organic amendments with a C/N ratio above ~30 (Hodge et al., 2000; Bonanomi et al., 2014).

5. Concluding remarks

Numerical simulations of hydrological processes and nitrate transport provide useful process-oriented indicators that can be integrated with the information retrieved from GIS-based approaches to map NVZs and quantify potential hazards of detrimental anthropogenic environmental impacts. The use of process-oriented models is often prevented by the lack of key measurements and farmers’ information (e.g., about irrigation and fertilization). Nevertheless, the use of numerical models

can be enhanced in the future by investing in monitoring network infrastructures. Effective soil hydraulic and nitrate transport parameters can be estimated using ad hoc inverse modeling procedures supported by available vadose zone data. The 20 years long model simulations show that agricultural practices strongly influence root nitrate uptake and nitrate leaching. In all cases, nitrate transit times are about two years to bypass the root zone and about 7–8 years to reach the shallow aquifer. Groundwater nitrate contamination is a consequence of nitrate leaching and will be subject to future investigations. The proposed approach can produce vulnerability maps for nitrate pollution or other pollutant types for other areas of the Campanian alluvial plain and other similar regions worldwide.

Declaration of Competing Interest

The authors declare that they have no known competing financial interests or personal relationships that could have appeared to influence the work reported in this paper.

Acknowledgments

The study reported in this paper was supported in part by Istituto Zooprofilattico Sperimentale del Mezzogiorno (IZSM) through the “Transparency in Campania” Action Plan, and MiUR-PRIN Project “WATER mixing in the critical ZONE: observations and predictions under environmental changes – WATZON” (grant 2017SL7ABC). We are grateful to the Managing Director of IZSM, Antonio Limone.

Appendix A. Supporting information

Supplementary data associated with this article can be found in the online version at doi:10.1016/j.agwat.2021.107208.

References

- Allen, R.G., Pereira, L.S., Raes, D., Smith, M., 1998. Crop evapotranspiration: guidelines for computing crop water requirements. Irrigation and Drainage Paper No. 56, Food and Agriculture Organization of the United Nations (FAO), Rome, Italy, 300p.
- Antonakos, A.K., Lambrakis, N.J., 2007. Development and testing of three hybrid methods for the assessment of aquifer vulnerability to nitrates, based on the drastic model, an example from NE Korinthia, Greece. *J. Hydrol.* 333, 288–304.
- Assouline, S., Or, D., 2014. The concept of field capacity revisited: defining intrinsic static and dynamic criteria for soil internal drainage dynamics. *Water Resour. Res.* 50 <https://doi.org/10.1002/2014WR015475>.
- Beegum, S., Šimůnek, J., Szymkiewicz, A., Sudheer, K.P., Nambi, I.M., 2018. Updating the Coupling Algorithm between HYDRUS and MODFLOW in the HYDRUS Package for MODFLOW. *Vadose Zone J.* 17 (1), 8. <https://doi.org/10.2136/vzj2018.02.0034> (180034).
- Beegum, S., Šimůnek, J., Szymkiewicz, A., Sudheer, K.P., Nambi, I.M., 2019. Implementation of solute transport in the vadose zone into the ‘HYDRUS package for MODFLOW’. *Groundwater* 57 (3), 392–408. <https://doi.org/10.1111/gwat.12815>.
- Bonanomi, G., D’Ascoli, R., Scotti, R., Gaglione, S.A., Caceres, M.G., Sultana, S., Rao, M., Zoina, A., 2014. Soil quality recovery and crop yield enhancement by combined application of compost and wood to vegetables grown under plastic tunnels. *Agric. Ecosyst. Environ.* 192, 1–7.
- Bonfante, A., Monaco, E., Manna, P., De Mascellis, R., Basile, A., Buonanno, M., Cantilena, G., Esposito, A., Tedeschi, A., De Michele, C., Belfiore, O., Catapano, I., Ludeno, G., Salinas, K., Brook, A., 2019. LCIS DSS—an irrigation supporting system for water use efficiency improvement in precision agriculture: a maize case study. *Agric. Syst.* 176, 102646.
- Boumaiza, L., Chesnaux, R., Walter, J., Stumpp, C., 2021. Constraining a flow model with field measurements to assess water transit time through a vadose zone. *Groundwater* 59, 417–427. <https://doi.org/10.1111/gwat.13056>.
- Braden, H., 1985. Ein Energiehaushalts- und Verdunstungsmodell für Wasser und Stoffhaushaltsuntersuchungen landwirtschaftlich genutzter Einzugsgebiete. *Mittel Dtsch. Bodenk. Gesellschaft* 42, 294–299.
- Bradshaw, J.K., Radcliffe, D.E., Šimůnek, J., Wunsch, A., McCray, J.E., 2013. Nitrogen fate and transport in a conventional onsite wastewater treatment system installed in a clay soil: a nitrogen chain model. *Vadose Zone J.* 12 (3), 20. <https://doi.org/10.2136/vzj2012.0150>.
- Busico, G., Mastrociccio, M., Cuoco, E., Sirna, M., Tedesco, D., 2019. Protection from natural and anthropogenic sources: a new rating methodology to delineate “Nitrate Vulnerable Zones”. *Environ. Earth Sci.* 78, 104. <https://doi.org/10.1007/s12665-019-8118-2>.

- Busico, G., Kazakis, N., Colombani, N., Khosravi, K., Voudouris, K., Mastrocicco, M., 2020. The importance of incorporating denitrification in the assessment of groundwater vulnerability. *Appl. Sci.* 10 (2328), 1–11.
- Cassa per il Mezzogiorno, 1983. *Idrogeologia dell'Italia Centro-Meridionale*. Quaderno nr. 4/2, Roma (in Italian).
- Catani, V., Zuzolo, D., Esposito, L., Albanese, S., Pagnozzi, M., Fiorillo, F., De Vico, B., Cicchella, D., 2020. A new approach for aquifer vulnerability assessment: the case study of Campania Plain. *Water Resour. Manag.* 34, 819–834. <https://doi.org/10.1007/s11269-019-02476-5>.
- Clausnitzer, V., Hopmans, J.W., Nielsen, D.R., 1992. Simultaneous scaling of soil water retention and hydraulic conductivity curves. *Water Resour. Res.* 28, 19–31.
- Corbari, C., Ben Charfi, I., Mancini, M., 2021. Optimizing irrigation water use efficiency for tomato and maize fields across Italy combining remote sensing data and the AquaCrop Model. *Hydrology* 8 (8), 39. <https://doi.org/10.3390/hydrology8010039>.
- De Vita, P., Allocca, V., Celico, F., Fabbrocino, S., Cesaria, M., Monacelli, G., Musilli, I., Piscopo, V., Scalise, A.R., Summa, G., Tranfaglia, G., Celico, P., 2018. Hydrogeology of continental southern Italy. *J. Maps* 14 (2), 230–241.
- Deb, S.K., Sharma, P., Shukla, M.K., Ashigh, J., Šimůnek, J., 2016. Numerical evaluation of nitrate distributions in the onion root zone under conventional furrow fertilization. *J. Hydrol. Eng.* 21 (2), 05015026 [https://doi.org/10.1061/\(ASCE\)HE.1943-5584.0001304](https://doi.org/10.1061/(ASCE)HE.1943-5584.0001304).
- Demurtas, C.E., Seddaiu, G., Ledda, L., Cappaia, C., Doro, L., Carletti, A., Roggero, P.P., 2016. Replacing organic with mineral N fertilization does not reduce nitrate leaching in double crop forage systems under Mediterranean conditions. *Agric. Ecosyst. Environ.* 219, 83–92.
- Doerfliger, N., Jeannin, P.Y., Zwahlen, F., 1999. Water vulnerability assessment in karst environments: a new method of defining protection areas using a multiattribute approach and GIS tools (EPIK method). *Environ. Geol.* 39, 165–176.
- Ducci, D., Della Morte, R., Mottola, A., Onorati, G., Pugliano, G., 2019. Nitrate trends in groundwater of the Campania region (southern Italy). *Environ. Sci. Pollut. Res.* 26, 2120–2131.
- Feddes, R.A., Kowalik, P.J., Zarandny, H., 1978. *Simulation of field water use and crop yield*. John Wiley & Sons, New York, NY.
- Fusco, F., Allocca, V., Coda, S., Cusano, D., Tufano, R., De Vita, P., 2020. Quantitative assessment of specific vulnerability to nitrate pollution of shallow alluvial aquifers by process-based and empirical approaches. *Water* 12 (1), 269. <https://doi.org/10.3390/w12010269>.
- Gómez-Hernández, J.J., Wen, X.-H., 1994. Probabilistic assessment of travel times in groundwater modeling. *Stoch. Hydrol. Hydraul.* 8, 19–55.
- Hanson, B.R., Šimůnek, J., Hopmans, J.W., 2006. Evaluation of urea–ammonium–nitrate fertigation with drip irrigation using numerical modeling. *Agric. Water Manag.* 86, 102–113.
- Hargreaves, G.H., Allen, R.G., 2003. History and evaluation of Hargreaves evapotranspiration equation. *J. Irrig. Drain. Eng.* 129 (1), 53–63. [https://doi.org/10.1061/\(ASCE\)0733-9437\(2003\)129:1\(53\)](https://doi.org/10.1061/(ASCE)0733-9437(2003)129:1(53)).
- Hodge, A., Robinson, D., Fitter, A., 2000. Are microorganisms more effective than plants at competing for nitrogen? *Trends Plant Sci.* 5, 304–308.
- Huan, H., Wang, J., Teng, Y., 2012. Assessment and validation of groundwater vulnerability to nitrate based on a modified DRASTIC model: a case study in Jilin City of northeast China. *Sci. Total Environ.* 440, 14–23.
- Infascelli, R., Pelorosso, R., Boccia, L., 2009. Spatial assessment of animal manure spreading and groundwater nitrate pollution. *Geospat. Health* 4 (1), 27–38.
- Li, Y., Šimůnek, J., Zhang, Z., Jing, L., Ni, L., 2015. Evaluation of nitrogen balance in a direct-seeded-rice field experiment using Hydrus-1D. *Agric. Water Manag.* 148, 213–222.
- Malik, W., Isla, R., Dechmi, F., 2019. DSSAT-CERES-maize modelling to improve irrigation and nitrogen management practices under Mediterranean conditions. *Agric. Water Manag.* 213, 298–308.
- Matteau, J.-P., Gumiere, S.J., Gallichand, J., Létourneau, G., Khiri, L., Gasser, M.-O., Michaud, A., 2019. Coupling of a nitrate production model with HYDRUS to predict nitrate leaching. *Agric. Water Manag.* 213, 616–626.
- Mattern, S., Vanlooster, M., 2010. Estimating travel time of recharge water through a deep vadose zone using a transfer function model. *Environ. Fluid Mech.* 10, 121–135.
- Matzeu, A., Secci, R., Uras, G., 2017. Methodological approach to assessment of groundwater contamination risk in an agricultural area. *Agric. Water Manag.* 184, 46–58.
- McLay, C.D.A., Dragten, R., Sparling, G., Selvarajah, N., 2001. Predicting groundwater nitrate concentrations in a region of mixed agricultural land use: a comparison of three approaches. *Environ. Pollut.* 115, 191–204.
- Miller, E.E., Miller, R.D., 1956. Physical theory for capillary flow phenomena. *J. Appl. Phys.* 27, 324–332.
- Millington, R.J., Quirk, J.M., 1961. Permeability of porous solids. *Trans. Faraday Soc.* 57, 1200–1207.
- Mokari, E., Shukla, M.K., Šimůnek, J., Fernandez, J.L., 2019. Numerical modeling of nitrate in a flood-irrigated pecan orchard. *Soil Sci. Soc. Am. J.* 83, 555–564.
- Mualem, Y., 1976. A new model for predicting the hydraulic conductivity of unsaturated porous media. *Water Resour. Res.* 12, 513–522.
- Mylevaganam, S., Ray, C., 2016. The assessment of groundwater vulnerability due to leaching of chemicals: the review of attenuation factor. *Open J. Soil Sci.* 6, 9–20.
- Nasta, P., Gates, J.B., 2013. Plot-scale modeling of soil water dynamics and impacts of drought conditions beneath rainfed maize in Eastern Nebraska. *Agric. Water Manag.* 128, 120–130.
- Nasta, P., Romano, N., 2016. Use of a flux-based field capacity criterion to identify effective hydraulic parameters of layered soil profiles subjected to synthetic drainage experiments. *Water Resour. Res.* 52 <https://doi.org/10.1002/2015WR016979>.
- Nasta, P., Romano, N., Assouline, S., Vrugt, J.A., Hopmans, J.W., 2013. Prediction of spatially-variable unsaturated hydraulic conductivity using scaled particle-size distribution functions. *Water Resour. Res.* 49 <https://doi.org/10.1002/wrcr.20255>.
- Nasta, P., Allocca, C., Deidda, R., Romano, N., 2020a. Assessing the impact of seasonal-rainfall anomalies on catchment-scale water balance components. *Hydrol. Earth Syst. Sci.* 24, 1–17.
- Nasta, P., Palladino, M., Sica, B., Pizzolante, A., Trifuoggi, M., Toscanesi, M., Giarra, A., D'Auria, J., Nicodemo, F., Mazzitelli, C., Lazzaro, U., Di Fiore, P., Romano, N., 2020b. Evaluating pedotransfer functions for predicting soil bulk density using hierarchical mapping information in Campania. *Geoderma Reg.* 21, e00267 <https://doi.org/10.1016/j.geodrs.2020.e00267>.
- Nasta, P., Szabó, B., Romano, N., 2021. Evaluation of Pedotransfer Functions for predicting soil hydraulic properties: A voyage from regional to field scales across Europe. *J. Hydrol. Reg. Stud.* 37 <https://doi.org/10.1016/j.ejrh.2021.100903>.
- National Research Council, 1993. *Ground Water Vulnerability Assessment: Contamination Potential under Conditions of Uncertainty*. National Academy Press, Washington, DC, USA.
- Panagopoulos, G.P., Antonakos, A.K., Lambrakis, N.J., 2006. Optimization of the DRASTIC method for groundwater vulnerability assessment via the use of simple statistical methods and GIS. *Hydrogeol. J.* 14, 894–911.
- Pelosi, A., Medina, H., Villani, P., D'Urso, G., Chirico, G.B., 2016. Probabilistic forecasting of reference evapotranspiration with a limited area ensemble prediction system. *Agric. Water Manag.* 178, 106–118.
- Perego, A., Basile, A., Bonfante, A., De Mascellis, R., Terribile, F., Brenna, S., Acutis, M., 2012. Nitrate leaching under maize cropping systems in Po Valley (Italy). *Agric. Ecosyst. Environ.* 147, 57–65. <https://doi.org/10.1016/j.agee.2011.06.014>.
- Piccini, C., Di Bene, C., Farina, R., Pennelli, B., Napoli, R., 2016. Assessing nitrogen use efficiency and nitrogen loss in a forage-based system using a modeling approach. *Agronomy* 6, 23. <https://doi.org/10.3390/agronomy6020023>.
- Prudic, D.E., Konikow, L.F., Bant, E.R., 2004. A new stream-flow routing (SFR1) package to simulate stream-aquifer interaction with MODFLOW-2000, U.S. Geological Survey Open-File Report 2004-1042, 95p.
- Ramos, T.B., Šimůnek, J., Gonçalves, M.C., Martins, J.C., Prazeres, A., Pereira, L.S., 2012. Two-dimensional modeling of water and nitrogen fate from sweet sorghum irrigated with fresh and blended saline waters. *Agric. Water Manag.* 111, 87–104. <https://doi.org/10.1016/j.agwat.2012.05.007>.
- Ritchie, J.T., 1972. Model for predicting evaporation from a row crop with incomplete cover. *Water Resour. Res.* 8, 1204–1213.
- Romano, N., Santini, A., 2002. Water retention and storage: field. In: Dane, J.H., Topp, G. C. (Eds.), *Methods of Soil Analysis, Part 4: Physical Methods*, SSSA Book Series N.5. Wiley, Madison, WI, USA, pp. 721–738. <https://doi.org/10.2136/sssabookser5.4.c26> (ISBN 0-89118-841-X).
- Rupert, M.G., 2001. Calibration of the DRASTIC Ground Water Vulnerability Mapping Method. *Ground Water* 39, 625–630.
- Sacchi, E., Acutis, M., Bartoli, M., Brenna, S., Delconte, C.A., Laini, A., Pennisi, M., 2013. Origin and fate of nitrates in groundwater from the central Po plain: insights from isotopic investigations. *Appl. Geochem.* 34, 164–180.
- Šimůnek, J., Hopmans, J.W., 2009. Modeling compensated root water and nutrient uptake. *Ecol. Model.* 220, 505–521.
- Šimůnek, J., Šejna, M., van Genuchten, M.T., 2016. Recent developments and applications of the HYDRUS computer software packages. *Vadose Zone J.* 15, 1–25. <https://doi.org/10.2136/vzj2016.04.0033>.
- Sprenger, M., Erhardt, M., Riedel, M., Weiler, M., 2016a. Historical tracking of nitrate in contrasting vineyards using water isotopes and nitrate depth profiles. *Agric. Ecosyst. Environ.* 222, 185–192.
- Sprenger, M., Seeger, S., Blume, T., Weiler, M., 2016b. Travel times in the vadose zone: variability in space and time. *Water Resour. Res.* 52, 5727–5754. <https://doi.org/10.1002/2015WR018077>.
- Stumpp, C., Stichler, W., Kandolf, M., Šimůnek, J., 2012. Effects of land cover and fertilization method on water flow and solute transport in five lysimeters: a long-term study using stable water isotopes. *Vadose Zone J.* 11 (1) <https://doi.org/10.2136/vzj2011.0075>.
- Szabó, B., Weynants, M., Weber, T.K., 2021. Updated European hydraulic pedotransfer functions with communicated uncertainties in the predicted variables (euptrfv2). *Geosci. Model Dev.* 14, 151–175.
- Tafteh, A., Sepaskhah, A.R., 2012. Application of HYDRUS-1D model for simulating water and nitrate leaching from continuous and alternate furrow irrigated rapeseed and maize fields. *Agric. Water Manag.* 113, 19–29. <https://doi.org/10.1016/j.agwat.2012.06.011>.
- Tufano, R., Allocca, V., Coda, S., Cusano, D., Fusco, F., Nicodemo, F., Pizzolante, A., De Vita, P., 2020. Groundwater vulnerability of principal aquifers of the Campania region (southern Italy). *J. Maps* 16, 565–576. <https://doi.org/10.1080/17445647.2020.1787887>.
- Turkeltaub, T., Ascott, M.J., Goody, D.C., Jia, X., Shao, M.-A., Binley, A., 2020. Prediction of regional-scale groundwater recharge and nitrate storage in the vadose zone: a comparison between a global model and a regional model. *Hydrol. Proc.* 34, 3347–3357. <https://doi.org/10.1002/hyp.13834>.
- Turkeltaub, T., Jia, X., Zhu, Y., Shao, M.-A., Binley, A., 2021. A comparative study of conceptual model complexity to describe water flow and nitrate transport in deep unsaturated Loess. *Water Resour. Res.* 57 <https://doi.org/10.1029/2020WR029250>.
- van Genuchten, M.T., 1980. A closed form equation for predicting the hydraulic conductivity of unsaturated soils. *Soil Sci. Soc. Am. J.* 44, 892–898.
- Van Stempvoort, D., Evert, L., Wassenaar, L., 1993. Aquifer vulnerability index: a GIS compatible method for groundwater vulnerability mapping. *Can. Water Resour. J.* 18, 25–37.

- Veizaga, E.A., Rodriguez, L., Ocampo, C.J., 2016. Investigating nitrate dynamics in a fine-textured soil affected by feedlot effluents. *J. Contam. Hydrol.* 193, 21–34.
- Vigliotti, M., Busico, G., Ruberti, D., 2020. Assessment of the vulnerability to agricultural nitrate in two highly diversified environmental settings. *Environments* 7, 80. <https://doi.org/10.3390/environments7100080>.
- Wall, D.P., Delgado, A., O'Sullivan, L., Creamer, R.E., Trajanov, A., Kuzmanovski, V., Bugge Henriksen, C., Debeljak, M., 2020. A decision support model for assessing the water regulation and purification potential of agricultural soils across Europe. *Front. Sustain. Food Syst.* 4, 115. <https://doi.org/10.3389/fsufs.2020.00115>.
- Weynants, M., Vereecken, H., Javaux, M., 2009. Revisiting Vereecken pedotransfer functions: introducing a closed-form hydraulic model. *Vadose Zone J.* 8 (1), 86–95. <https://doi.org/10.2136/vzj2008.0062>.
- Wösten, J.H.M., Lilly, A., Nemes, A., Le Bas, C., 1999. Development and use of a database of hydraulic properties of European soils. *Geoderma* 90, 169–185.
- Zeng, J., Yang, J., Zha, Y., Shi, L., 2019. Capturing soil-water and groundwater interactions with an iterative feedback coupling scheme: new HYDRUS package for MODFLOW. *Hydrol. Earth Syst. Sci.* 23, 637–655. <https://doi.org/10.5194/hess-23-637-2019>.